

Mechanism of Force Generation of a Viral DNA Packaging Motor

Yann R. Chemla,^{1,7} K. Aathavan,^{2,7}
Jens Michaelis,^{1,4,8} Shelley Grimes,⁵
Paul J. Jardine,⁵ Dwight L. Anderson,^{5,6}
and Carlos Bustamante^{1,2,3,4,*}

¹Department of Physics

²Biophysics Graduate Group

³Department of Molecular and Cell Biology and
Department of Chemistry

⁴Howard Hughes Medical Institute
University of California, Berkeley
Berkeley, California 94720

⁵Department of Oral Science

⁶Department of Microbiology
University of Minnesota
Minneapolis, Minnesota 55455

Summary

A large family of multimeric ATPases are involved in such diverse tasks as cell division, chromosome segregation, DNA recombination, strand separation, conjugation, and viral genome packaging. One such system is the *Bacillus subtilis* phage ϕ 29 DNA packaging motor, which generates large forces to compact its genome into a small protein capsid. Here we use optical tweezers to study, at the single-molecule level, the mechanism of force generation in this motor. We determine the kinetic parameters of the packaging motor and their dependence on external load to show that DNA translocation does not occur during ATP binding but is likely triggered by phosphate release. We also show that the motor subunits act in a coordinated, successive fashion with high processivity. Finally, we propose a minimal mechanochemical cycle of this DNA-translocating ATPase that rationalizes all of our findings.

Introduction

The genomes of many double-stranded DNA bacteriophages and certain animal viruses, such as herpesvirus and adenovirus, are packaged into a preformed protein precursor capsid (prohead) to near-crystalline density (Jardine and Anderson, 2006). This process is driven by a molecular motor that utilizes energy derived from ATP hydrolysis. The *Bacillus subtilis* bacteriophage ϕ 29 is an excellent system to investigate the DNA packaging mechanism because both robust bulk (Grimes et al., 2002) and single-viral-particle packaging assays (Smith et al., 2001) exist.

The advent of single-molecule manipulation techniques has allowed, for the first time, the direct investigation of the mechanochemical processes during packaging. In

a previous study (Smith et al., 2001), force-measuring optical tweezers were used to follow individual ϕ 29 packaging complexes in real time. The highly processive motor can package the 19.3 kbp genome against loads as high as 57 pN, its stall force, and, as the prohead is filled beyond 50% of its capacity, an internal force due to DNA confinement builds, reaching intracapsid pressures of 60 atm (Smith et al., 2001). This pressure may be used during infection to inject the DNA into a host cell (Smith et al., 2001; Gonzalez-Huici et al., 2004; Evilevitch et al., 2003).

The molecular motor of ϕ 29 is comprised of three components: (1) the head-tail connector, a dodecamer of the gene 10 product (gp10), which is situated at the base of the prolate icosahedral prohead and has a channel through which DNA is translocated (Simpson et al., 2000; Guasch et al., 2002); (2) a ring comprised of five (Simpson et al., 2000; Morais et al., 2001) or six (Zhang et al., 1998; Guo et al., 1998) copies of the 174 nucleotide ϕ 29-encoded prohead RNA (pRNA) (Guo et al., 1987a) bound to the connector (Grimes et al., 2002); and (3) multiple copies of the RNA-dependent packaging ATPase gp16 (Simpson et al., 2000; Grimes and Anderson, 1990; Shu and Guo, 2003). The gp16 ATPases are arranged in a ring-like structure oriented coaxially and in direct contact with the pRNA ring, and they likely operate as gp16-pRNA heterodimers (Grimes et al., 2002).

The mechanism of DNA packaging is still poorly understood. The ϕ 29 motor is among the strongest motors known, generating \sim 10 times more force than kinesin and \sim 25 times more force than myosin. It is of considerable interest to understand the design principles that allow this motor to generate high mechanical forces with very high efficiencies and at high processivity. Moreover, it is of great interest to understand how the motor converts the chemical free energy from ATP hydrolysis into mechanical work. This understanding requires the study of the mechanochemistry of the molecular motor, involving the characterization of the chemical and mechanical work cycles (Bustamante et al., 2004). Single-molecule manipulation techniques such as optical tweezers that can measure and apply forces on individual molecules are especially well suited for such studies. Here we use single-molecule and bulk biochemical assays to (1) characterize the kinetic parameters of the packaging motor, (2) investigate the mechanism of coordination among the motor subunits, (3) determine the dependence of the kinetic parameters on the external load to identify the force-generating steps in the mechanochemical cycle of the motor, and (4) arrive at a minimal mechanism consistent with motor operation.

Results

ATP Dependence of Packaging Rate

We begin our analysis with measurements of the packaging rate at various ATP concentrations, in order to

*Correspondence: carlos@alice.berkeley.edu

⁷These authors contributed equally to this work.

⁸Present address: Department Chemie, Ludwig-Maximilians Universität München, D-81377 München, Germany.

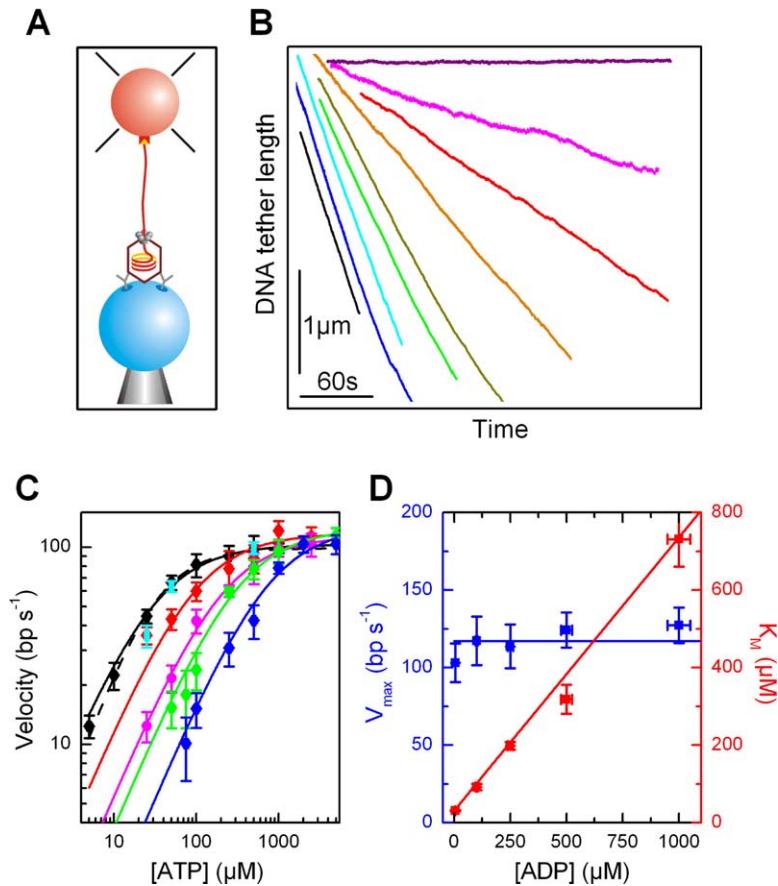


Figure 1. Dependence of Packaging Rate on ATP, ADP, and P_i Concentration

(A) Experimental configuration (not to scale). A stalled complex forms a tether between a microsphere (red) in an optical trap and a microsphere (blue) on a micropipette (Smith et al., 2001) (see Experimental Procedures).

(B) Representative packaging traces measured at a constant force of ~ 5 pN showing the DNA tether length plotted against time for nine packaging complexes under different conditions: [ATP] = 1000, 500, 250, 100, 50, 25, 10, and 5 μM and stalled (black, dark blue, cyan, green, yellow ochre, orange, red, magenta, and violet, respectively); [ADP] = [P_i] = 5 μM . The traces are offset for clarity.

(C) Mean packaging rate plotted against ATP concentration for different ADP and P_i concentrations: [ADP] = 5, 100, 250, 500, and 1000 μM with [P_i] = 5 μM (black, red, magenta, green, and blue); [ADP] = 5 μM with [P_i] = 5000 μM (cyan). Each data point represents the average of the mean velocities from an ensemble of individual traces ($n = 4-39$) measured at constant force ~ 5 pN. Error bars in packaging rates were given by the standard deviations from each ensemble. Nonlinear least-square fits to the Michaelis-Menten equation (solid lines) and the Hill equation (dashed black line) are shown.

(D) V_{max} (blue axis) and K_M (red axis) as determined from the fits in (C), plotted against [ADP]; solid lines are fits to the competitive-inhibition model described in the text.

better understand the ATP binding process. In our experiment, a single stalled packaging complex was attached between a microsphere in an optical trap and a microsphere placed on the end of a micropipette (Figure 1A and Experimental Procedures). Figure 1B shows typical traces of individual packaging events where DNA outside the prohead decreases in length over time as it is reeled into the capsid against a constant external force of ~ 5 pN. ATP concentrations range from 5 to 1000 μM , with ADP and inorganic phosphate (P_i) fixed at 5 μM each (the latter added to ensure a defined free energy of hydrolysis, $\Delta G = \Delta G^0 + k_B T \ln([ATP]/[ADP][P_i])$).

The average packaging velocity calculated from such traces is plotted against ATP concentration in the black curve of Figure 1C and follows the Michaelis-Menten equation (solid curve):

$$v = V_{\text{max}} \frac{[ATP]}{K_M + [ATP]} \quad (1)$$

yielding a maximum velocity $V_{\text{max}} = 103 \pm 12 \text{ bp s}^{-1}$, and $K_M = 31 \pm 2 \mu\text{M}$. (Strictly speaking, Equation 1 should be corrected to account for the reverse reaction: $v = V_{\text{max}} ([ATP] - [ADP][P_i]/K_{\text{eq}})/(K_M + [ATP])$, where $K_{\text{eq}} [> 10^{11} \mu\text{M}]$ is the equilibrium constant for ATP hydrolysis. For the range of product concentrations used in this paper ([ADP] = 5–1000 μM , [P_i] = 5–5000 μM), this correction is insignificant.) A fit to the more general Hill

equation $v = V_{\text{max}} [ATP]^n / (K_M^n + [ATP]^n)$ (dashed curve, Figure 1C) yields a Hill coefficient close to unity ($n = 1.2 \pm 0.2$). This result implies that either (1) each ATPase subunit can bind ATP and generate a step completely independently of each other, i.e., there is no binding cooperativity or coordination between the ATPases or (2) for every step, one or more ATPases can bind ATP successively and in coordination but not cooperatively (Schnitzer and Block, 1997). A Hill coefficient of 1 does not mean that the motor can only bind one ATP per mechanochemical cycle or that a single ATP is bound to the motor at any given time. Rather, it implies that the binding of one ATP neither facilitates nor hinders the binding of another ATP.

Previous bulk measurements (Guo et al., 1987b) confirmed presently (see Experimental Procedures) show that DNA is translocated by 2 base pairs (0.68 nm) per ATP hydrolyzed. Thus, if the motor were to bind n ATP molecules per step, it would translocate the DNA by $n \times 2$ base pairs. Although our data cannot rule out a mechanism with $n > 1$ at this point, we favor the most parsimonious model, in which the motor binds one ATP and translocates the DNA by 2 base pairs per catalytic cycle.

Effect of ADP and Phosphate

Next, to study the process of product release, we investigated the effect of ADP and P_i on the packaging

velocity. As shown in [Figure 1C](#), increasing the P_i concentration 1000-fold (to 5 mM) had no discernable effect on the packaging velocity at several ATP concentrations and at a constant force of ~ 5 pN. This result indicates that the equilibrium constant for phosphate release is very large and that the release step may be considered irreversible. [Figure 1C](#) also shows substrate-saturation curves measured at ADP levels ranging from 5 μM to 1 mM. Fits to [Equation 1](#) reveal that K_M increases with ADP, whereas V_{max} remains constant ([Figure 1D](#)). These curves were also fit to a Hill equation. The Hill coefficients did not significantly differ from unity ($n = 1.2 \pm 0.2$ for $[\text{ADP}] = 5 \mu\text{M}$, $n = 0.7 \pm 0.5$ at 100 μM , $n = 1.0 \pm 0.1$ at 250 μM , $n = 1.2 \pm 0.2$ at 500 μM , and $n = 1.3 \pm 0.3$ at 1 mM; on average, $n = 1.05 \pm 0.25$). This result is consistent with ADP acting as a competitive inhibitor to ATP. Since the inhibitor may always be outcompeted by the addition of more substrate, V_{max} is independent of inhibitor concentration. On the other hand, K_M increases with inhibitor concentration because a progressively larger amount of substrate is required to counter the inhibitory effects. The data ([Figure 1D](#)) are well described by a competitive-inhibition model ([Segel, 1975](#)), with $K_M = K_M^0(1 + [\text{ADP}]/K_D)$, where $K_M^0 = 30 \pm 9 \mu\text{M}$ is the Michaelis-Menten constant at $[\text{ADP}] = 0$ and the binding constant for ADP, $K_D = 44 \pm 13 \mu\text{M}$. The linear dependence on ADP concentration indicates that the inhibition involves binding of only one ADP molecule at the active site. As shown below, these results limit the classes of mechanisms consistent with motor operation.

Packaging with Nonhydrolyzable ATP Analogs

To investigate the coordination between motor subunits during packaging, we blocked the hydrolysis cycle by supplementing the ATP buffer with variable amounts of the nonhydrolyzable ATP analog AMP-PNP, which reversibly stalls packaging in bulk (unpublished data). [Figure 2A](#) shows traces obtained for individual proheads packaging at a constant external load of ~ 5 pN, at a fixed ATP concentration of 100 μM ($[\text{ADP}] = [\text{P}_i] = 5 \mu\text{M}$), and at AMP-PNP concentrations in the range of 0–5 μM . In the presence of AMP-PNP, packaging is interrupted by pauses ($\gg 1$ s), yet the velocity between pauses is not affected ([Figure 2A](#)). The motor also pauses in the absence of AMP-PNP ([Smith et al., 2001](#)), but inherent pauses are less frequent and of shorter duration than the pauses induced here and were excluded from this analysis. The frequency of induced pauses, i.e., the number of pauses per length of DNA packaged, increases linearly with the amount of AMP-PNP for a given concentration of ATP ([Figure 2B](#)). The pause duration is not affected by AMP-PNP concentration (see [Figure S1](#) in the [Supplemental Data](#) available with this article online). These results indicate that the binding of only one AMP-PNP to the motor is sufficient to cause a pause. If more than one AMP-PNP molecule ($n > 1$) had to bind to induce a pause, the frequency would vary with a power-law dependence (i.e., as $[\text{AMP-PNP}]^n$). We also find that the pause frequency decreases inversely with ATP for a given concentration of AMP-PNP ([Figure 2C](#)). This dependence implies that AMP-PNP binds to the motor in competi-

tion with ATP. Also, the pause duration is not affected by the ATP concentration ([Figure S1](#)). These experiments were repeated with another ATP analog, $\gamma\text{S-ATP}$, revealing the same qualitative behavior ([Figure S2](#)). Taken together, these observations show that binding of a single nonhydrolyzable ATP analog to the active site, in competition with ATP, is sufficient to stall the motor for a duration corresponding to the residence time of the analog on the motor.

The above results allow us to better understand the coordination between subunits of the motor. Two possible conclusions may be derived. One is that the actions of the ATPases are coordinated and interdependent such that blocking the hydrolysis cycle of one ATPase brings the entire motor to a halt. The other possibility is that despite the motor being a multimer, only one subunit is continuously active, and the pauses are the result of blocking the chemical cycle of that subunit. However, previous studies using pRNA mutants demonstrate the involvement of all pRNAs during packaging ([Trottier et al., 1996](#); [Chen and Guo, 1997](#)), favoring the former scenario. These results, combined with a Hill coefficient of 1, mean that the ATPases cannot be independent but must act in succession: that is, each ATPase must finish its mechanochemical cycle before the next can complete its own. This conclusion need not mean that the firing order is ordinal (i.e., 1 2 3 4 5 1 2 3... around the ring of ATPases); it can even be random or nonordinal (e.g., 1 3 5 2 4 1 3...).

Interestingly, competitive inhibition by ADP did not result in observable pauses in packaging. Presumably the release rates and binding rates of ADP to the motor are sufficiently fast that pauses are exceedingly short-lived and are not detected by our methods.

Packaging under Load

Next we investigated the force dependence of the packaging velocity in order to decipher the coordination between the mechanical and chemical steps. The packaging rate v and the ATP turnover rate k_{ATP} of the motor are related by: $v(F) = \epsilon d \cdot k_{\text{ATP}}$, where d is the step size and ϵ is the coupling coefficient, i.e., the probability that the motor steps per hydrolysis cycle. The dependence of the packaging velocity on applied load may be explained if the partitioning between productive and futile hydrolyses depends on force, leading to a load-dependent coupling coefficient $\epsilon(F)$. Alternatively, the force dependence may result from one or more load-dependent steps in the cycle, resulting in a force-dependent ATP turnover rate $k_{\text{ATP}}(F)$. The force dependence of the Michaelis-Menten parameters V_{max} and K_M can be used to distinguish between these alternatives ([Visscher et al., 1999](#)) and, in the latter case, also identify the location of the force-dependent transitions within the hydrolysis cycle ([Keller and Bustamante, 2000](#)).

DNA packaging rates were monitored as a function of force at ATP concentrations ranging from 10 to 500 μM ([Figure 3A](#)) and at high and low ADP and phosphate concentrations ([Figure 3B](#)). In these measurements, the load applied by the optical trap on the motor increases as the DNA is packaged, until the motor stalls (see [Experimental Procedures](#)). The data is well described by a single force-dependent transition with an Arrhenius-

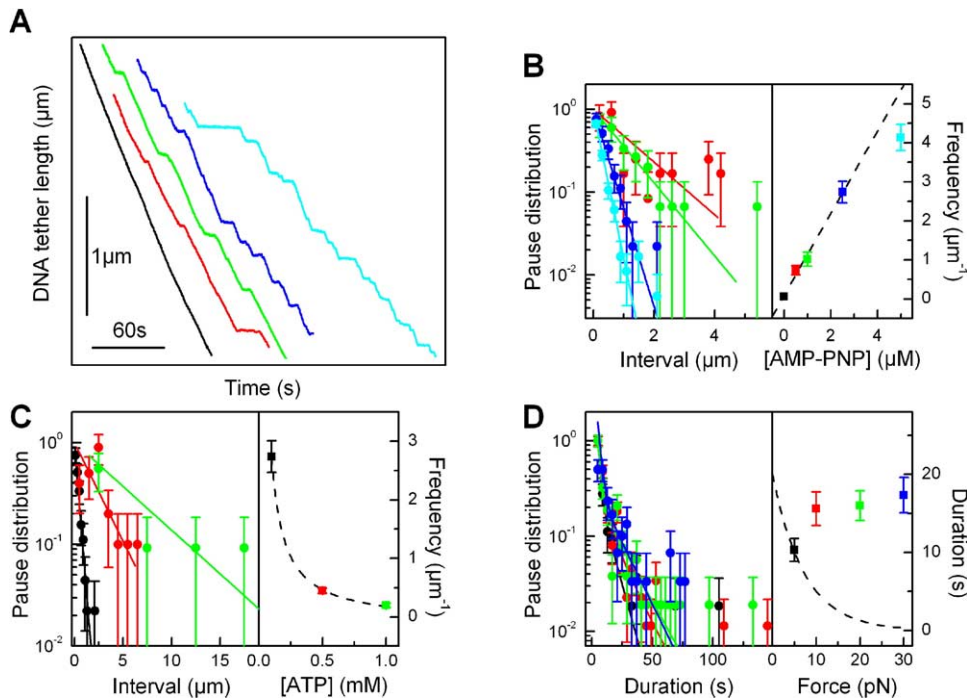


Figure 2. Pauses Induced by AMP-PNP

(A) Packaging traces at a constant force of ~ 5 pN and $[ATP] = 100 \mu\text{M}$, $[ADP] = [P_i] = 5 \mu\text{M}$ as a function of AMP-PNP concentration: $[AMP\text{-}PNP] = 0, 0.5, 1, 2.5,$ and $5 \mu\text{M}$ (black, red, green, blue, and cyan, respectively). The traces are offset for clarity.

(B) Normalized distribution of the pause interval versus $[AMP\text{-}PNP]$: color coding same as in (A) (number of pauses $n = 1, 37, 36, 89,$ and 210 , respectively). For $[AMP\text{-}PNP] = 0$, only one pause longer than 3 s was observed in $\sim 20 \mu\text{m}$ of total packaging. Solid lines show fits to an exponential distribution. Inset: mean frequency (pauses per μm packaged) from fit versus $[AMP\text{-}PNP]$; dashed line is a linear fit to the data. The data point at $[AMP\text{-}PNP] = 5 \mu\text{M}$ (cyan) possibly undercounts pauses, as they are frequent enough that two or more may be counted as one, and was excluded from the fit. The frequency $\sim [AMP\text{-}PNP]/(d \cdot \kappa [ATP])$, where κ is the ratio of the docking rates of ATP and AMP-PNP to the motor. The slope of the fit yields $\kappa = 14 \pm 0.9$.

(C) Normalized distribution of the pause interval versus ATP concentration: $[ATP] = 100, 500,$ and $1000 \mu\text{M}$ (black, red, and green); $[AMP\text{-}PNP] = 2.5 \mu\text{M}$ and $F = 5$ pN ($n = 89, 24,$ and 10 , respectively). Inset: mean frequency versus $[ATP]$; data fitted to an inverse law (dashed line), which yields $\kappa = 13 \pm 1.3$.

(D) Normalized distribution of the pause duration versus force: $F = 5, 10, 20,$ and 30 pN (black, red, green, and blue); $[AMP\text{-}PNP] = 2.5 \mu\text{M}$, $[ATP] = 100 \mu\text{M}$, and $[ADP] = [P_i] = 5 \mu\text{M}$ ($n = 89, 193, 114,$ and 58 , respectively). Data were fit to a biexponential distribution (solid lines). Rare, extremely long-duration pauses are observed in the tails of the distributions. These tails may be due to the binding of additional AMP-PNP to the motor or due to multiple pauses counted as one. Inset: mean pause duration versus force. Error bars are the standard error of the mean. Dashed line shows duration predicted for a force-dependent AMP-PNP binding step. Error bars in all distribution plots were obtained from the square root of the number of pausing events in each bin.

like dependence, $\exp(-F\Delta x/k_B T)$, where $\Delta x = 0.11$ nm (Smith et al., 2001). Here, Δx is a “characteristic distance” corresponding to the distance along the mechanical reaction coordinate to the transition state (Smith et al., 2001). At near-saturating ATP levels ($[ATP] \gg K_M$), the packaging rate, and thus the rate-limiting step, depends strongly on force. In this regime, $v \approx V_{\text{max}} = \epsilon d \cdot k_{\text{cat}}$, where k_{cat} is an “effective” catalytic constant that depends on several microscopic rate constants. However, at low ATP concentrations ($[ATP] < K_M$), where the rate-limiting step is ATP binding and its commitment to hydrolysis, the velocity becomes force independent. In this regime, the packaging velocity $v \approx V_{\text{max}}[ATP]/K_M = \epsilon d \cdot k_b [ATP]$, where $k_b = V_{\text{max}}/(\epsilon d \cdot K_M)$ is an effective second-order binding constant (Visscher et al., 1999). Fitting the data in Figure 3A to Equation 1 reveals that V_{max} and K_M decrease with load at the same rate (Figure 3C), so that their ratio $V_{\text{max}}/K_M = \epsilon d \cdot k_b$ is indeed force independent (Figure 3D).

Phosphate has no effect on the force-velocity behav-

ior of the motor (Figure 3B) as would be expected if phosphate release were irreversible. The effect of ADP on the force-velocity behavior of the motor (Figure 3B) is consistent with ADP binding with a force-independent rate constant (see Supplemental Data).

Coupling between Mechanical and Chemical Cycles

The force independence of V_{max}/K_M rules out models with a load-dependent coupling efficiency $\epsilon(F)$ (Visscher et al., 1999). Those models predict that both $V_{\text{max}} = \epsilon(F)d \cdot k_{\text{cat}}$ and $V_{\text{max}}/K_M = \epsilon(F)d \cdot k_b$ should be force dependent, whereas $K_M = k_{\text{cat}}/k_b$ should be force independent, contrary to our observations. “Mixed” coupling models, with one or more load-dependent steps in the hydrolysis cycle in addition to a load-dependent coupling coefficient $\epsilon(F)$, predict that V_{max} , K_M , and V_{max}/K_M will all depend on force, again inconsistent with our results.

Instead, the data show that the force dependence of the packaging rate results from a load-dependent step

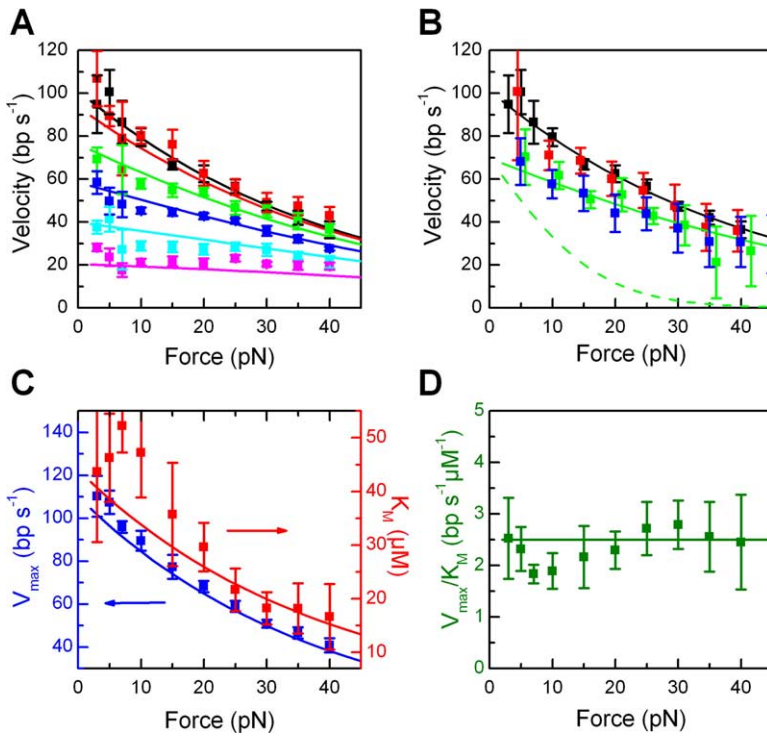


Figure 3. Dependence of Packaging Rate on Force

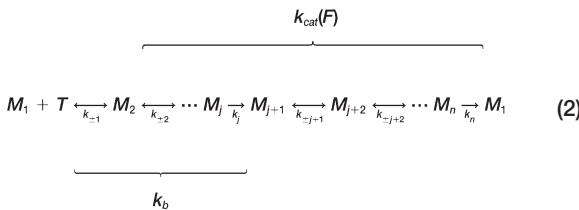
(A) Force-velocity behavior at various ATP concentrations: [ATP] = 500, 250, 100, 50, 25, and 10 μM (black, red, green, blue, cyan, and pink, respectively); [ADP] = [P_i] = 5 μM. Individual traces that reached loads of 40 pN (n = 6–20 traces) were selected and averaged together in 5 pN bins. Error bars are obtained from the standard deviations at each force. Solid lines are determined from the fits in (C) and (D) and the model described in the text and the Supplemental Data.

(B) Force-velocity behavior at [ATP] = 500 μM and high and low ADP and P_i concentrations: [ADP] = 5 μM (black) and 500 μM ADP (green) with [P_i] = 5 μM in both; [ADP] = 5 μM and [P_i] = 5000 μM (red); [ADP] = 500 μM and [P_i] = 500 μM (blue). The solid green line is determined from a model with a reversible, force-independent ADP release step; the dashed green line is obtained for a force-dependent ADP release step (see Supplemental Data).

(C) V_{max} (blue) and K_M (red) as determined from fits of the data in (A) to the Michaelis-Menten equation, plotted against force.

(D) The ratio V_{max}/K_M, plotted against force. Error bars are obtained from the fits. Solid lines in (C) and (D) are based on the model in the text and the Supplemental Data.

in the hydrolysis cycle of the motor. Moreover, the data require not only that the catalytic rate $k_{cat}(F)$ be load dependent but that the effective binding rate k_b not be, restricting which transitions in the cycle coincide with the force-dependent DNA translocation. The following scheme shows a generic cycle of a motor that binds one molecule of ATP:



where $M_1 \dots M_n$ are the states of the motor and $k_{\pm 1} \dots k_n$ are the kinetic rate constants (k_1 is the rate constant of the forward transition from state 1 to 2, and k_{-1} is the rate constant of the reverse transition from state 2 to 1, etc.). In this scheme, ATP binding is modeled as a second-order “docking” step in which ATP comes into loose contact with the catalytic cleft, followed by a first-order step in which ATP becomes more tightly bound (Keller and Bustamante, 2000). It can be shown (see Supplemental Data) that, for this scheme, k_{cat} depends on the rate constants of all transitions except that of the ATP docking step (i.e., $k_{\pm 2}, k_{\pm 3} \dots k_n$, in scheme 2). On the other hand, k_b depends on the rate constants of all steps connected by a reversible path to the ATP docking step up to and including the first irreversible step to follow docking (i.e., $k_{\pm 1}, k_{\pm 2} \dots k_j$). Therefore, the observed force independence of k_b requires that the force-dependent step must follow the

first irreversible step after ATP docking (step j), between steps $j+1$ and n (i.e., $k_{\pm j+1}, k_{\pm j+2} \dots k_n$).

The force independence of k_b rules out a scheme where ATP docking powers translocation. A scheme in which force generation occurs during the tight binding of ATP, as suggested for F₁-ATPase (Oster and Wang, 2000), is also inconsistent with our data. Since docking is likely reversible, the force independence of k_b rules out a subsequent tight binding transition as a force-generating step.

Force Dependence of Pauses

There is yet another method to rule out the tight binding of ATP as the translocation step. This method is based on the fact that the long duration of pauses induced by AMP-PNP requires that the binding of this analog involve not only a docking step but also the formation of a long-lived, tightly bound state similar to that of ATP. If ATP tight binding coincided with translocation and thus were force dependent, a force applied on DNA should promote the unbinding of ATP. Therefore, the effect of the tension on the DNA should be to decrease the ATP release time and hence the duration of the AMP-PNP-induced pauses as $\exp[F(d - \Delta x)/k_B T]$. While the docking rates for ATP and AMP-PNP differ by a factor of ~14 (Figure 2B) (the docking rates for ATP and γ S-ATP are almost identical; see Figure S2), we expect the force dependence of the binding event to be similar. Accordingly, the pause duration should decrease ~40-fold with an increase in external force of 25 pN. Instead, we observed no decrease in pause duration in the force range 5–30 pN (Figure 2D).

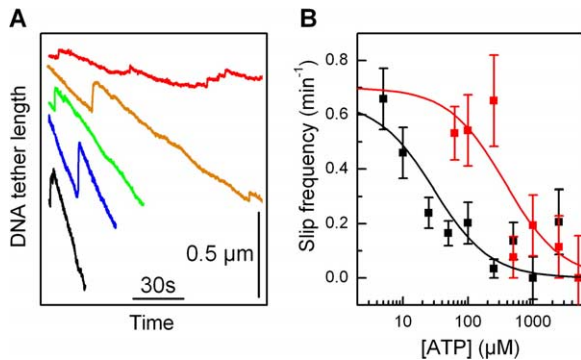


Figure 4. Slipping-Frequency Dependence on Nucleotide Concentration

(A) Representative time traces of slipping events at various ATP concentrations: [ATP] = 500, 100, 25, 10, and 5 μM (black, dark blue, green, orange, and red, respectively); [ADP] = [P_i] = 5 μM . The traces are offset for clarity.

(B) Slipping frequency (slips per minute of packaging) at a constant force of ~ 5 pN as a function of ATP and ADP concentration. Data at various ADP concentrations were binned into two sets: low ADP (5, 100, and 250 μM , black), and high ADP (500 and 1000 μM , red). The slipping frequency f_s was modeled as the sum of the slipping rates in the nucleotide-free and ADP-docked states, $k_{s,E}$ and $k_{s,ADP}$, multiplied by their respective probabilities: $f_s \approx (k_{s,E} + k_{s,ADP} [\text{ADP}]/K_D) \cdot K_M^0 / (K_M^0 (1 + [\text{ADP}]/K_D) + [\text{ATP}])$ (see Supplemental Data). Solid lines show fits to this model. The only fitting parameters were the slipping rates $k_{s,E}$ and $k_{s,ADP}$; the values of K_M^0 and K_D were taken from the fits in Figure 1D (see text). The fits yield $k_{s,E} = 0.64 \pm 0.12 \text{ min}^{-1}$ and $k_{s,ADP} = 0.69 \pm 0.10 \text{ min}^{-1}$. Error bars were obtained from the square root of the number of slipping events at each nucleotide concentration.

Nucleotide Dependence of Motor-DNA Interaction

Since the motor generates high forces, it should be tightly engaged to DNA during translocation. It also follows that part of the motor must at some point disengage from the DNA in order to reposition itself for the next translocation cycle. Thus, determining the DNA affinity of the motor in its different nucleotide bound states can help understand the coordination between translocation and the hydrolysis cycle.

The $\phi 29$ motor displays occasional slips in packaging (Figure 4A), which result from temporary detachments of the motor from the DNA. We use these events as a direct probe for the DNA affinity of the motor. Figure 4B shows the slipping frequency, defined as the number of slips per time, as a function of nucleotide concentration and at a constant force of ~ 5 pN. At low ADP (5–250 μM , black curve in Figure 4B), the slipping frequency increases from 0 as ATP is lowered below K_M . At high ADP (500 and 1000 μM , red curve in Figure 4B), this increase in slipping frequency also occurs, but at higher ATP concentrations than at low ADP. These results establish that the nucleotide state of the motor affects its affinity to DNA. The observed dependence of the slip rate on [ATP] and [ADP] is well described by the probability that the active subunit is empty or ADP bound multiplied by the intrinsic slipping rates from those states (see Supplemental Data), indicating that the affinity of the active site for DNA is low in the empty or ADP bound states. Finally, since the slipping frequency is negligible at high [ATP] at both ADP levels, the ATP bound state must have a high affinity for DNA.

To confirm this interpretation, we have also developed an assay for motor-DNA affinity based on zonal-rate sedimentation in sucrose density gradients (see Experimental Procedures). In this experiment, the affinity of the motor for various nucleotide bound states is determined from the leakage of prepackaged DNA from the capsid of packaging intermediates in different nucleotide conditions—the ATP analogs $\gamma\text{S-ATP}$ and AMP-PNP, the hydrolysis transition-state analog ADP vanadate, and ADP. Any DNA that leaks out of the capsid adds to its hydrodynamic drag, causing the particle to sediment more slowly; the greater the leakage, the larger the drag.

Stalled complexes run into gradients containing 0.4 μM $\gamma\text{S-ATP}$ sediment to a position (peak at fraction #4 in Figure 5A) corresponding to complexes that fully retain their DNA. Identical results are obtained in gradient buffers containing 5 μM AMP-PNP and 500 μM ADP vanadate. However, in gradients containing no nucleotides or containing ADP, complexes sediment into a long tail corresponding to extensive leakage of DNA (Figure 5A). Although the exact shape of the sedimentation profile depends upon the velocity of DNA exit, the rate of disengagement from the DNA, and the rate of exchange of nucleotides into the gradient buffer, these results indicate that the motor has a weak DNA affinity in the absence of nucleotides or in the presence of ADP, in agreement with the slipping data (Figure 4B).

Varying the gradient $\gamma\text{S-ATP}$ concentration, we observe two phases to the sedimentation profiles of stalled complexes (Figure 5B). At low [$\gamma\text{S-ATP}$] ($< 0.4 \mu\text{M}$), the number of filled capsids increases with $\gamma\text{S-ATP}$ concentration, as expected since the motor has a higher DNA affinity when bound to $\gamma\text{S-ATP}$ than in the absence of nucleotides. However, as $\gamma\text{S-ATP}$ is increased beyond 0.4 μM , the complexes sediment more slowly, indicative of partial DNA leakage (Figure 5B). This biphasic behavior suggests that the motor is capable of binding more than one $\gamma\text{S-ATP}$ and that the DNA affinity of the motor is affected not just by the nucleotide state of one subunit but by that of two or more subunits. The motor appears to have two types of binding sites for $\gamma\text{S-ATP}$: one that binds $\gamma\text{S-ATP}$ strongly and is responsible for the first phase ([$\gamma\text{S-ATP}$] $< 0.4 \mu\text{M}$), in which DNA is engaged tightly to the motor, and a second that binds $\gamma\text{S-ATP}$ weakly and is responsible for the second phase ([$\gamma\text{S-ATP}$] $> 0.4 \mu\text{M}$), in which DNA is less tightly engaged to the motor (see Figure S3). Since DNA leakage is used as a reporter in our assay, we cannot observe nucleotide binding events that do not affect the motor-DNA interaction. Thus, other subunits may be empty or may bind nucleotides in a fashion independent of the motor's affinity to DNA. The reduced affinity observed at high nucleotide concentration is also seen with AMP-PNP but, interestingly, not with ADP vanadate. This latter observation suggests that the motor is in this reduced-DNA-affinity configuration only when it has bound two nonhydrolyzed ATP molecules.

Discussion

A minimal mechanochemical cycle for the motor that rationalizes all of the above results can now be proposed. In Figure 6A, we follow the hydrolysis pathway

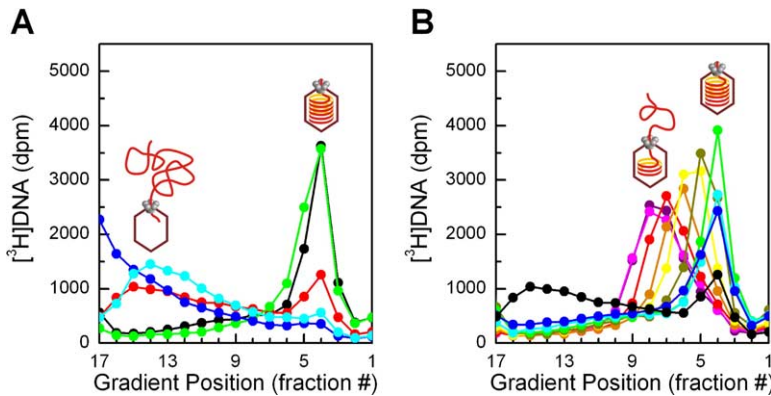


Figure 5. Nucleotide Dependence of Motor-DNA Affinity

(A) Sedimentation profiles (left to right) of packaging intermediates containing [³H]DNA. The black and red curves correspond to particles stalled with 250 μM γS-ATP and then diluted into gradients with γS-ATP (0.4 μM) and no nucleotides, respectively. The green, blue, and cyan curves are experiments where particles were stalled with 500 μM ADP vanadate and run into a gradient with ADP vanadate, no nucleotides, and ADP, respectively. (B) Sedimentation profiles of particles stalled with 250 μM γS-ATP and run into gradients with [γS-ATP] = 0, 0.025, 0.1, 0.4, 1.7, 6.4, 16, 40, 100, and 250 μM (black, dark blue, cyan, green, yellow ochre, yellow, orange, red, magenta, and purple, respectively).

for a single ATPase subunit in which we summarize the conclusions of the nucleotide-dependent motor-DNA affinity. Since each ATPase spends a portion of its cycle disengaged from the DNA and the motor is highly processive, DNA translocation must involve at least two subunits. The activities of these two ATPases must be coordinated such that at least one is engaged to the DNA at every step in the mechanochemical cycle of the motor. This conclusion is corroborated by the observation that the nucleotide state of at least two subunits affects the affinity of the motor for DNA and the coordination of the ATPase subunits implied by the AMP-PNP pausing data. Furthermore, the reduced DNA affinity of the motor in the presence of multiple nonhydrolyzed ATPs and its high processivity require that, during its normal operation, at least one subunit either is bound to a hydrolyzed ATP molecule or is empty. Thus, the overall mechanochemical cycle of the entire motor must involve the overlap of at least two of the cycles

shown in Figure 6A, satisfying the requirement that at least one subunit remain engaged with the DNA at all times and that only one subunit be engaged with the DNA during the translocation step. In Figure 6B, we propose an overall cycle consisting of six mechanochemical steps involving two subunits.

In constructing this model, we used the following constraints obtained from the data. (1) The force independence of k_b requires that the movement step follow the first irreversible step after ATP docking; that irreversible step is likely to be the tight binding of ATP (Step II in Figure 6B), as suggested by the long duration of the analog-induced pauses. The rate constant k_{TB} for tight binding must be much larger than $k_{cat} = 50 \text{ s}^{-1}$ since it is not the rate-limiting translocation step; the rate constant for the reverse transition (from tightly to loosely bound) k_{-TB} is extremely small, on the order of 0.1 s^{-1} , as given by the inverse of the mean analog-induced-pause duration. Thus, $k_{TB}/k_{-TB} \gg 500$ (or

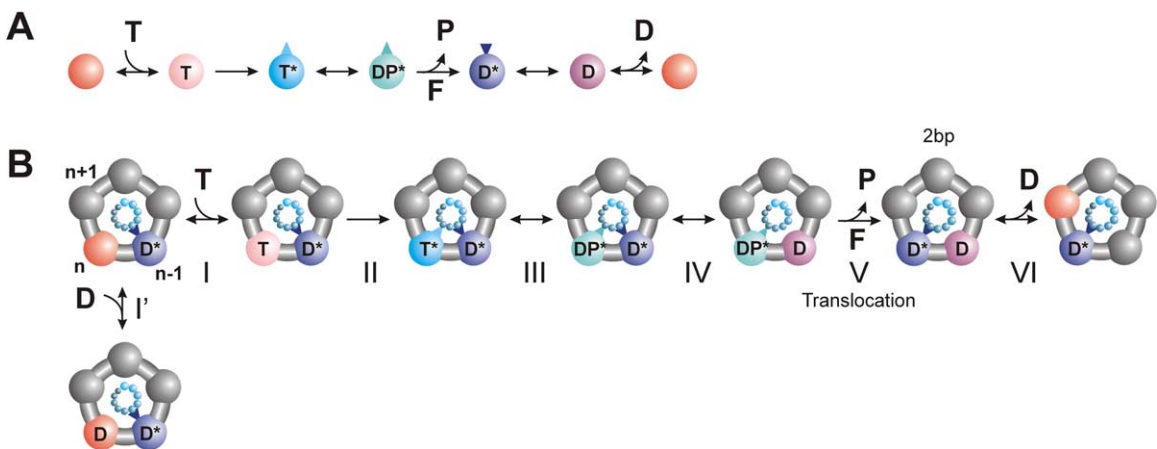


Figure 6. Putative Minimal Mechanochemical Scheme

(A) The dominant pathway of each ATPase consists of six steps. An empty subunit (red sphere) docks ATP (T, pink). ATP becomes tightly bound (T^* , blue), and the subunit engages with the DNA (denoted by blue triangle). After hydrolysis (DP^* , cyan), phosphate is released (D^* , dark blue), and DNA is translocated (upturned dark-blue triangle). DNA disengages (D, purple), and ADP is released.

(B) In the mechanochemical cycle of the entire motor, the subunits must be coordinated such that the motor maintains contact with the DNA at every step. The DNA (light blue, only one strand shown for simplicity) translocates by 2 bp out of the page during the force-generating step (V). Two alternate mechanisms for competitive ADP inhibition are shown: on pathway (VI) or off pathway (I'). ATPases not directly involved in the translocation cycle are shown in gray; the state of these subunits is independent of the mechanochemical cycle and may be empty or nucleotide bound. Although the model shows five subunits, it may be extended to six with no loss of generality.

$\Delta G_{TB} > 6 k_B T$), and the tight binding transition can be considered irreversible. (2) Phosphate release (Step V) is also irreversible since the packaging velocity is not affected even at a high concentration of $[P_i] = 5000 \mu\text{M}$. Thus, the equilibrium constant for phosphate release $k_P/k_{-P} \gg 5000 \mu\text{M}$ (or $\Delta G_P > 7k_B T$ for $[P_i] = 5 \mu\text{M}$). (3) ADP is a competitive inhibitor, indicating that ADP and ATP bind to the same state of the motor. If inhibition occurs in an on-pathway process, ADP binds to the motor in a reverse of the release process (Step VI), which must immediately precede the subsequent ATP binding event (Step I). Alternatively, ADP may bind in an off-pathway process (Step I'), unrelated to the release step, to a "dead-end" state. In this case, ADP release on the main pathway (Step VI) may be irreversible, and it may not immediately precede ATP binding. (4) Force generation most likely occurs during product release, which comprises the large free-energy change essential for a power stroke. For this motor, the movement step can generate forces as high as 57 pN, translocating DNA over 2 bp = 0.68 nm, corresponding to an equilibrium constant of 2×10^4 or a free-energy change of 10 $k_B T$. Such a large free-energy change is unlikely to occur during hydrolysis, which only involves a small rotation of the terminal phosphate (Oster and Wang, 2000). In the case that ADP release is irreversible and ADP inhibits the motor through an off-pathway state, the movement step must precede or coincide with either ADP or P_i release. In the case that ADP inhibition is on pathway, ADP release must follow that of P_i . The equilibrium constant for ADP release $k_D/k_{-D} = 44 \mu\text{M}$ (or $\Delta G_D \sim 2 k_B T$ for $[\text{ADP}] = 5 \mu\text{M}$), which is insufficient for the power stroke. Furthermore, the observed force-velocity behavior of the motor at high ADP concentration (Figure 3B) is inconsistent with a force-dependent ADP release. Thus, we believe the most likely scenario is that the movement step occurs upon P_i release.

In Figure 6B (and Movie S1), the motor is shown as a ring of five ATPases, each of which can adopt one of the six mechanochemical states. ATP docks (Step I) to a subunit in the ring denoted n ; the previous subunit $n-1$ has completed its translocation cycle and is still engaged with DNA. ATP then binds tightly (Step II), as subunit n engages DNA, and hydrolyzes (Step III). The latter triggers the disengagement of DNA from the previous subunit $n-1$ (Step IV), completing the transfer of DNA from one subunit to the next, followed by DNA translocation triggered by the release of phosphate (Step V). Finally, ADP is released (Step VI) from subunit $n-1$, returning the motor to its original conformation, rotated by one. In the subsequent cycle, ATP docks to the next ATPase in the ring, $n+1$. The state of the other subunits (marked in gray) is independent of the mechanochemical cycle and may be empty or nucleotide bound.

More complex schemes are possible if one considers a greater number of chemical and conformational states. In particular, models in which more than one ATP binds the motor and more than one 2 bp translocation step occurs per mechanochemical cycle have not been considered. In addition, the exact nature of the conformational changes in the motor components—namely, the gp16 ATPase, the pRNA ring, and the connector—involved in DNA translocation is not addressed

here. However, our model is general enough to accommodate such structural information when available.

We assume a sequential order of firing around the ATPase ring as the simplest scenario. However, a non-ordinal or random firing order is also a viable mechanism consistent with our results. Using optical tweezers, it may be possible to distinguish between random and sequential firing of the ATPases by studying motors containing one mutant subunit functioning at a slower rate than the wild-type. Also, considering that the helical pitch of B-DNA is ~ 10.5 bp/turn, the step size of the motor is 2 bp, and the motor is pentameric or hexameric, rotation between the motor and DNA may be necessary to bring the next subunit in register with the DNA for each step. This analysis implies that the phage DNA packaging motor's cycle must involve force and torque components that may be investigated by simultaneously applying force and torque to the DNA as it is packaged, a subject of current research.

The $\phi 29$ packaging motor ATPase is related to the FtsK-HerA superfamily of ATPases, which in turn is related to the larger AAA class of ATPases (Iyer et al., 2004; L. Aravind, personal communication). F_1 -ATPase is one molecular motor in this large family whose mechanochemistry has been well characterized. In F_1 -ATPase, the transition from loosely to tightly bound ATP occurs in a zippering of hydrogen bonds—the "binding zipper"—which induces elastic strain in the catalytic subunit and produces the first of two force-generating power strokes driving the motor. A second power stroke occurs when that elastic strain is relieved in a recoil step triggered by P_i release and immediately preceding ADP release (Oster and Wang, 2000). The $\phi 29$ packaging motor appears to share parts of the mechanism of F_1 -ATPase. Here we believe that the ATP binding step cocks the motor and the DNA-translocation power stroke occurs during the recoil of the motor triggered by P_i release. Interestingly, a similar mechanism linking force generation to a posthydrolytic step has been proposed recently for the ssRNA packaging protein P4 of the phage $\phi 12$, based on crystallographic studies (Mancini et al., 2004).

We have obtained here, using force-measuring optical tweezers, the first detailed mechanochemical cycle of a viral DNA packaging machine and, in general, of a DNA-translocating ATPase. The FtsK-HerA superfamily of ATPases to which the $\phi 29$ motor is related plays a central role in many important cellular activities such as cell division, chromosome segregation, recombination, strand separation, and conjugation (Iyer et al., 2004). Our findings should be of immediate relevance to such DNA-translocating ATPases that are now studied with increasing interest using single-molecule techniques (Dawid et al., 2004; Saleh et al., 2004; Pease et al., 2005), as a similar mechanism of force generation may be expected for these systems.

Experimental Procedures

Optical-Trap Measurements

Proheads were partially packaged with biotinylated DNA-gp3 and stalled with γ S-ATP, a nonhydrolyzable ATP analog. Tethers were formed between a streptavidin-coated microsphere in an optical trap and an anti-phage-antibody-coated microsphere placed on

the end of a micropipette. Packaging was initiated inside the experimental chamber containing packaging buffer (described below) in flow. Measurements were carried out in two modes: “constant force feedback,” in which the distance between the microspheres was adjusted to maintain a constant tension in the DNA, and “no feedback,” in which the distance between the optical trap and the pipette was held constant. See [Smith et al. \(2001\)](#) for a complete description.

The packaging buffer consisted of 50 mM Tris-HCl (pH 7.8), 50 mM NaCl, and 5 mM MgCl₂ supplemented with ATP, ADP, and NaH₂PO₄ (a source of inorganic phosphate, P_i) in concentrations ranging from 5–5000 μM as detailed in the text. In the pausing experiments, AMP-PNP (0.5–5 μM, as specified in the text) and γS-ATP (50–500 nM, see [Figure S2](#)) were added to this buffer. The percentage error in ATP concentration was estimated to be ~5% as determined from measurements of inorganic phosphate from residual hydrolysis in our ATP buffers (Enz-Check Phosphate Assay Kit, Molecular Probes).

Data Analysis

Packaging-Rate Determination

Using the measured extension and force, the instantaneous contour length of the DNA tether was calculated from the worm-like chain model with a persistence length of $P = 53$ nm and a stretch modulus of $S = 1200$ pN·nm ([Baumann et al., 1997](#)). Packaging velocities were determined from a linear fit of the contour length over a sliding time window of size Δt . The choice of window size was dictated by noise considerations. Typically, we used windows ranging from 1.4 s (100 data points) at the highest velocities to 11.4 s (800 pts.) at the lowest. Drifts in the machine were reasonably low over the measurement times (see [Figure 1A](#)). We estimate the drifts to be <0.3 bp s⁻¹.

Average packaging rates were calculated only from data obtained at filling ratios smaller than ~50% (corresponding to DNA tether lengths greater than ~1.5 μm) to eliminate the effects of internal pressure. Under such conditions, the maximum internal force is less than 3 pN, which reduces the average packaging rate by less than 7% at saturating ATP levels ([Smith et al., 2001](#)). The motor occasionally exhibits slips and pauses. Both were removed prior to packaging-rate analysis because these events are most likely off the main kinetic pathway of the motor.

Pause Assignment

Data collected in constant-force-feedback mode were analyzed using the procedure outlined below. The contour length of the DNA tether measured as a function of time was binned (size $\Delta\ell$), and the times spent in each bin were determined. From a histogram of these “residence times,” a probability distribution was constructed representing the probability that the packaging motor resides in a bin of length $\Delta\ell$ for a time t .

For a motor that does not pause, such a distribution has an expected mean residence time $\langle t \rangle = \Delta\ell/v$, where v is the mean velocity, and a variance $\langle t^2 \rangle - \langle t \rangle^2$ determined by the Poisson fluctuations in packaging velocity and instrumental noise. On the other hand, a bin containing a pause has a significantly longer residence time, falling outside of the range expected from such a distribution. A confidence parameter can be ascribed to points in a distribution constructed from a particular data set to determine if they belong to the expected distribution for a nonpausing enzyme. Pauses in our data were assigned by selecting bins that we determined with 99% confidence to fall outside this distribution. To minimize the effect of instrumental noise, which was typically ~10 bp at our measurement bandwidth of ~70 Hz and at a force of ~5 pN, bins of length $\Delta\ell > 10$ bp were used to analyze the data. In the analysis of analog-induced pauses, inherent pauses were removed by excluding all pauses shorter than 3 s.

Data collected in no-feedback mode were analyzed using the procedure described ([Smith et al., 2001](#)).

Slip Determination

Packaging velocities were determined as described above from data collected in constant-force-feedback mode with DNA tether lengths greater than ~1.5 μm. A sliding time window of 2.8 s (200 data points) was used to calculate the velocity. Slips were selected according to a velocity threshold, typically set at -20 bp/s. Slips were usually longer than ~20 nm.

Step-Size Determination

An earlier bulk biochemical assay ([Guo et al., 1987b](#)) reported that the DNA is translocated by ~2 bp per ATP hydrolyzed. However, a great majority of the gp16 ATPase in those experiments did not form active, packaging complexes. The background ATPase activity of gp16 not involved in packaging may have led to an overestimation of the amount of ATP hydrolyzed during packaging and thus an underestimation of the distance of DNA translocated per ATP. We repeated this measurement using gp16 on proheads in approximately stoichiometric amounts.

The DNA-gp3, gp16, and proheads were purified as described in [Grimes and Anderson \(1997\)](#). For in vitro DNA packaging, uniformly-labeled [³H]DNA-gp3 and 15 copies of gp16 per prohead were mixed and incubated for 5 min in 1.5× packaging buffer (37.5 mM Tris [pH 7.8], 7.5 mM MgCl₂, and 75 mM NaCl). The prohead and gp16 ratios were determined by titration to be limiting for DNA translocation. One aliquot was removed to serve as a “no packaging” (no ATP) control. A second aliquot was removed and treated with 10 μg/ml of DNase I for 10 min before ATP addition and incubation (see below). ATP was added to 500 μM to the remainder of the reaction to initiate packaging, samples were drawn at 4 min, and packaging was stalled by the addition of 250 μM γS-ATP. Unpackaged DNA “tails” were digested by adding DNase I to 1 μg/ml and incubation for 5 min. Samples were centrifuged into 5%–20% sucrose density gradients in 1.5× packaging buffer with 1 μM γS-ATP in the SW55 rotor (Beckman) at 35,000 rpm for 30 min to isolate the partially filled heads. Total base pairs of DNA-gp3 packaged was quantified from the ³H per DNA mass and by determining the [³H]DNA in particles in gradient fractions by liquid scintillation counting. Total [³H]DNA in the gradients was normalized to [³H]DNA in the no-ATP control gradient. ATP hydrolysis was quantified in parallel by measuring generation of inorganic phosphate in the same packaging and control mixtures by the Lanzetta malachite green assay ([Lanzetta et al., 1979](#)) and by reference to a standard phosphate curve.

Background ATP hydrolysis due to components not engaged in packaging was quantified by phosphate generation in both a prohead/gp16 mixture without DNA and a complete packaging mixture treated with DNase I prior to ATP addition (see above). Phosphate generated in each of these mixtures (less than 5% of that produced in packaging) was subtracted independently from the values of phosphate measured during packaging. Four independent measurements of the step size yielded an average value of 1.99 ± 0.14 bp when subtracting a background from a prohead/gp16 mixture without DNA and $d = 2.02 \pm 0.19$ bp when subtracting a background from a DNase I-treated packaging mixture. Both values are in excellent agreement with the previous result. In these experiments, 31%–35% of the input DNA was packaged, ~1/2 that of the DNA packaged under optimal conditions (~70% input DNA packaged). This drop was due to the limiting prohead concentration used and the change in buffer conditions to suppress prohead/gp16 background ATPase activity.

Zonal-Rate Sucrose-Gradient Sedimentation

[³H]DNA-gp3, proheads, and gp16 were mixed in a 1:2:20 molar ratio, and packaging was initiated by the addition of ATP to 500 mM. At 5–6 min, packaging was stalled by the addition of 250 μM γS-ATP. DNase I was added to 1 μg/ml to digest the unpackaged right ends of DNA, and the mixture was incubated for 5 min. A 10 μl aliquot of the reaction mixture was diluted with 125 μl of packaging buffer (25 mM Tris [pH 7.8], 50 mM NaCl, and 5 mM MgCl₂) containing the appropriate nucleotide or analog. The sample was then centrifuged into a 5–20% linear sucrose density gradient containing packaging buffer with or without the nucleotide in the SW55 rotor at 35,000 rpm for 30 min at 20°C. Fractions were collected, and [³H]DNA-gp3 was quantified by liquid scintillation counting. Packaging complexes that retained [³H]DNA-gp3 in the prohead formed a rapidly sedimenting peak centering on fractions 4–5. In contrast, packaging complexes that were losing DNA had a more slowly sedimenting profile with a broad distribution of [³H]DNA-gp3 in fractions 10–17 ([Bjornsti et al., 1983](#)).

Supplemental Data

Supplemental Data include Supplemental Experimental Procedures, Supplemental References, three figures, and one movie

and can be found with this article online at <http://www.cell.com/cgi/content/full/122/5/683/DC1/>.

Acknowledgments

We thank S.B. Smith, D.E. Smith, S.J. Tans, N.R. Forde, Z.D. Bryant, S. Dumont, J. Gore, J. Erzberger, J. Berger, O. Igoshin, J.-C. Liao, G. Oster, and L. Aravind for helpful discussion. This research was supported in part by grants from NIH GM-071552 (C.B.), NIH DE-03606 (D.L.A.), NIH GM-059604 (S.G.), DOE DE-AC03-76DF00098 (C.B.), and the Packard Foundation 1999-8325 (C.B.). Y.R.C. is supported by a National Research Service Award fellowship from NIH GM-65786 and a Career Award at the Scientific Interface from the Burroughs Wellcome Fund. K.A. is supported by the Program in Mathematics and Molecular Biology through a Burroughs Wellcome Fund fellowship.

Received: February 2, 2005

Revised: May 12, 2005

Accepted: June 23, 2005

Published: September 8, 2005

References

- Baumann, C.G., Smith, S.B., Bloomfield, V.A., and Bustamante, C. (1997). Ionic effects on the elasticity of single DNA molecules. *Proc. Natl. Acad. Sci. USA* **94**, 6185–6190.
- Bjornsti, M.-A., Reilly, B.E., and Anderson, D.L. (1983). Morphogenesis of bacteriophage phi29 of *Bacillus subtilis*: oriented and quantized in vitro packaging of DNA protein gp3. *J. Virol.* **45**, 383–396.
- Bustamante, C., Chemla, Y.R., Forde, N.R., and Izhaky, D. (2004). Mechanical processes in biochemistry. *Annu. Rev. Biochem.* **73**, 705–748.
- Chen, C., and Guo, P.X. (1997). Sequential action of six viral encoded DNA packaging RNAs during the phage phi29 genomic DNA translocation. *J. Virol.* **71**, 3864–3871.
- Dawid, A., Croquette, V., Grigoriev, M., and Heslot, F. (2004). Single-molecule study of RuvAB-mediated Holliday junction migration. *Proc. Natl. Acad. Sci. USA* **101**, 11611–11616.
- Evilevitch, A., Lavelle, L., Knobler, C.M., Raspaud, E., and Gelbart, W.M. (2003). Osmotic pressure inhibition of DNA ejection from phage. *Proc. Natl. Acad. Sci. USA* **100**, 9292–9295.
- Gonzalez-Huici, V., Salas, M., and Hermoso, J.M. (2004). The push-pull mechanism of bacteriophage phi29 DNA injection. *Mol. Microbiol.* **52**, 529–540.
- Grimes, S., and Anderson, D.L. (1990). RNA dependence of the bacteriophage phi29 DNA packaging ATPase. *J. Mol. Biol.* **215**, 559–566.
- Grimes, S., and Anderson, D.L. (1997). The bacteriophage phi29 packaging proteins supercoil the DNA ends. *J. Mol. Biol.* **266**, 901–914.
- Grimes, S., Jardine, P.J., and Anderson, D.L. (2002). Bacteriophage phi29 DNA packaging. *Adv. Virus Res.* **58**, 255–294.
- Guasch, A., Pous, J., Ibarra, B., Gomis-Ruth, F.X., Valpuesta, J.M., Sousa, N., Carrascosa, J.L., and Coll, M. (2002). Detailed architecture of a DNA translocating machine: the high-resolution structure of the bacteriophage phi29 connector particle. *J. Mol. Biol.* **315**, 663–676.
- Guo, P.X., Erickson, S., and Anderson, D.L. (1987a). A small viral RNA is required for in vitro packaging of bacteriophage phi29 DNA. *Science* **236**, 690–694.
- Guo, P.X., Peterson, C., and Anderson, D.L. (1987b). Prohead and DNA-gp3-dependent ATPase activity of the DNA packaging protein gp16 of bacteriophage phi29. *J. Mol. Biol.* **197**, 229–236.
- Guo, P., Zhang, C., Chen, C., Garver, K., and Trottier, M. (1998). Inter-RNA interaction of phage phi29 pRNA to form a hexameric complex for viral DNA transportation. *Mol. Cell* **2**, 149–155.
- Iyer, L.M., Makarova, K.S., Koonin, E.V., and Aravind, L. (2004). Comparative genomics of the Ftsk-HerA superfamily of pumping ATPases: implications for the origins of chromosome segregation, cell division and viral capsid packaging. *Nucleic Acids Res.* **32**, 5260–5279.
- Jardine, P.J., and Anderson, D.L. (2006). DNA packaging in the bacteriophages. In *The Bacteriophages*, R. Calendar, ed. (New York: Oxford University Press), in press.
- Keller, D., and Bustamante, C. (2000). The mechanochemistry of molecular motors. *Biophys. J.* **78**, 541–556.
- Lanzetta, P.A., Alvarez, L.J., Reinach, P.S., and Candia, O.A. (1979). An improved assay for nanomole amounts of inorganic phosphate. *Anal. Biochem.* **100**, 95–97.
- Mancini, E.J., Kainov, D.E., Grimes, J.M., Tuma, R., Bamford, D.H., and Stuart, D.I. (2004). Atomic snapshots of an RNA packaging motor reveal conformational changes linking ATP hydrolysis to RNA translocation. *Cell* **118**, 743–755.
- Morais, M.C., Tao, Y., Olson, N.H., Grimes, S., Jardine, P.J., Anderson, D.L., Baker, T.S., and Rossmann, M.G. (2001). Cryo-electron-microscopy image reconstruction of symmetry mismatches in bacteriophage phi29. *J. Struct. Biol.* **135**, 38–46.
- Oster, G., and Wang, H. (2000). Reverse engineering a protein: the mechanochemistry of ATP synthase. *Biochim. Biophys. Acta* **1458**, 482–510.
- Pease, P.J., Levy, O., Cost, G.J., Gore, J., Ptacin, J.L., Sherratt, D., Bustamante, C., and Cozzarelli, N.R. (2005). Sequence-directed DNA translocation by purified FtsK. *Science* **307**, 586–590.
- Saleh, O.A., Perals, C., Barre, F.X., and Allemand, J.F. (2004). Fast, DNA-sequence independent translocation by FtsK in a single-molecule experiment. *EMBO J.* **23**, 2430–2439.
- Schnitzer, M.J., and Block, S.M. (1997). Kinesin hydrolyses one ATP per 8-nm step. *Nature* **388**, 386–390.
- Segel, I.H. (1975). *Enzyme Kinetics* (New York: Wiley & Sons), pp. 100–141.
- Shu, D., and Guo, P. (2003). Only one pRNA hexamer but multiple copies of the DNA-packaging protein gp16 are needed for the motor to package bacterial virus phi29 genomic DNA. *Virology* **309**, 108–113.
- Simpson, A.A., Tao, Y., Leiman, P.G., Badasso, M.O., He, Y., Jardine, P.J., Olson, N.H., Morais, M.C., Grimes, S., Anderson, D.L., et al. (2000). Structure of the bacteriophage phi29 DNA packaging motor. *Nature* **408**, 745–750.
- Smith, D.E., Tans, S.J., Smith, S.B., Grimes, S., Anderson, D.L., and Bustamante, C. (2001). The bacteriophage phi29 portal motor can package DNA against a large internal force. *Nature* **413**, 748–752.
- Trottier, M., Zhang, C., and Guo, P.X. (1996). Complete inhibition of virion assembly in vivo with mutant procapsid RNA essential for phage phi29 DNA packaging. *J. Virol.* **70**, 55–61.
- Visscher, L., Schnitzer, M.J., and Block, S.M. (1999). Single kinesin molecules studies with a molecular force clamp. *Nature* **400**, 184–188.
- Zhang, F., Lemieux, S., Wu, X., St.-Arnaud, D., McMurray, C.T., Major, F., and Anderson, D.L. (1998). Function of hexameric RNA in packaging of bacteriophage phi29 DNA. *Mol. Cell* **2**, 141–147.